THE ASTROPHYSICAL JOURNAL, 519:864–875, 1999 July 10

ON THE ORIGIN OF IMPULSIVE ELECTRON EVENTS OBSERVED AT 1 AU

SÄM KRUCKER, DAVIN E. LARSON, AND ROBERT P. LIN
Space Sciences Laboratory, University of California, Berkeley, Berkeley, CA 94720-7450; krucker@ssl.berkeley.edu
AND
BARBARA J. THOMPSON
Space Applications Corporation, NASA Goddard Space Flight Center, Greenbelt, MD
Received 1998 December 16; accepted 1999 February 15

ABSTRACT

A statistical survey of 12 impulsive electron events detected at energies down below 1 keV and 58 events detected above 25 keV observed at 1 AU by the 3-D Plasma and Energetic Particles experiment on the *Wind* spacecraft is presented. Timing analysis of the velocity dispersion reveals two different kinds of electron events: (1) events released from the Sun at the onset of a radio type III burst, which suggest that these electrons are part of the population producing the type III radio emission; and (2) events in which the electrons are released up to half an hour later than the onset of the type III burst. These electrons therefore may be produced by a different acceleration mechanism than the population producing the radio emission. Both types of behavior can be observed during the same impulsive electron event at different energies, but most events show the same timing at all energies. At lower energies (<25 keV), type III–related impulsive electron events are more often observed (nine of 12 events), whereas at higher energies (>25 keV), events not related to type III bursts are more numerous (41 of 58). However, events of both classes are observed below 1 keV. Impulsive electron events not related to type III radio bursts are observed to be proton rich, with an order-of-magnitude lower electron-to-proton ratio than events related to type III bursts.

For roughly 3/4 of the events not related to type III bursts, large-scale coronal transient waves, also called EIT waves or coronal Moreton waves, are observed by the Extreme Ultraviolet Imaging Telescope (EIT) on board *SOHO*. Temporal and spatial correlations together with hydromagnetic simulations show that at least some impulsive electron events are more likely related to the propagating Moreton wave than to the flare phenomenon itself.

Subject headings: Sun: flares — Sun: particle emission — Sun: radio radiation — Sun: X-rays, gamma rays

1. INTRODUCTION

The solar wind electron population shows a core ($kT \approx 10$ eV), a halo ($kT \approx 80$ eV; Feldman et al. 1975), and a superhalo ($kT > 1$ keV) component (D. E. Larson 1998, private communication). Superimposed on these quasi–steady state populations are solar impulsive electron events. The term "impulsive" is used here to describe the impulsive onset of the observed electron event; it does not necessarily indicate a short duration of the related solar soft X-ray (SXR) burst in the same way that "impulsive" is used to distinguish between solar energetic particle (SEP) events related to short-duration SXR bursts (impulsive SEP events) and long-duration SXR bursts (gradual SEP events) (cf. Reames 1995, 1997). Impulsive electron events are important diagnostics of particle acceleration at the Sun. A clear identification of the solar origin of these events observed at 1 AU is their velocity dispersion: Higher energy electrons need less time to travel from the Sun to 1 AU than lower energy ones. Therefore, the electron flux of solar events rises earlier at high energies than at lower energies. Impulsive electron events showing power-law spectra have been observed in the energy range from several MeV down to ≈ 0.5 keV (Lin 1985; Lin et al. 1996). The low cutoff energy indicates that at least the lower energy electrons must be released at high altitude in the solar corona (about $1\,R_\odot$ above the photosphere).

Impulsive electron events are very often flare-related, and about 90% of all events are accompanied by radio type III bursts (Lin 1985; Ergun et al. 1998). It is generally accepted that radio type III bursts are produced by electrons escaping from the Sun into the interplanetary space. The velocity dispersion of the escaping electrons can lead to a bump-on-tail electron beam unstable to the generation of Langmuir waves. These waves then are converted to the observed transverse radiation by different proposed mechanisms. The energies of unstable electrons in a beam are between 2 and 30 keV, as derived from radio observations and in situ detections.

The *Wind* 3-D Plasma and Energetic Particle experiment on the spacecraft (Lin et al. 1995) has a good temporal resolution for comparing the timing of impulsive electron events observed at 1 AU with radio type III bursts and solar flares in general. Timing analysis of a single event has been published by Ergun et al. (1998). They find a good agreement for the onset time of the type III bursts and the extrapolated energy release time at the Sun of the energetic electrons observed at 1 AU. However, the instruments on the *Wind* spacecraft also detect electron events showing an obvious delay of the release of the electrons from the type III burst onset. In addition, although one would expect that the footpoints of the field lines connecting the Sun and the spacecraft to be located at western longitudes, some of the observed impulsive electron events are clearly related to flares occurring in the east. In those events, the escape from the flare site to the spacecraft is difficult to explain.

Here we present statistical surveys that investigate the temporal and spatial association of impulsive electron events and radio type III bursts. Since most of the events

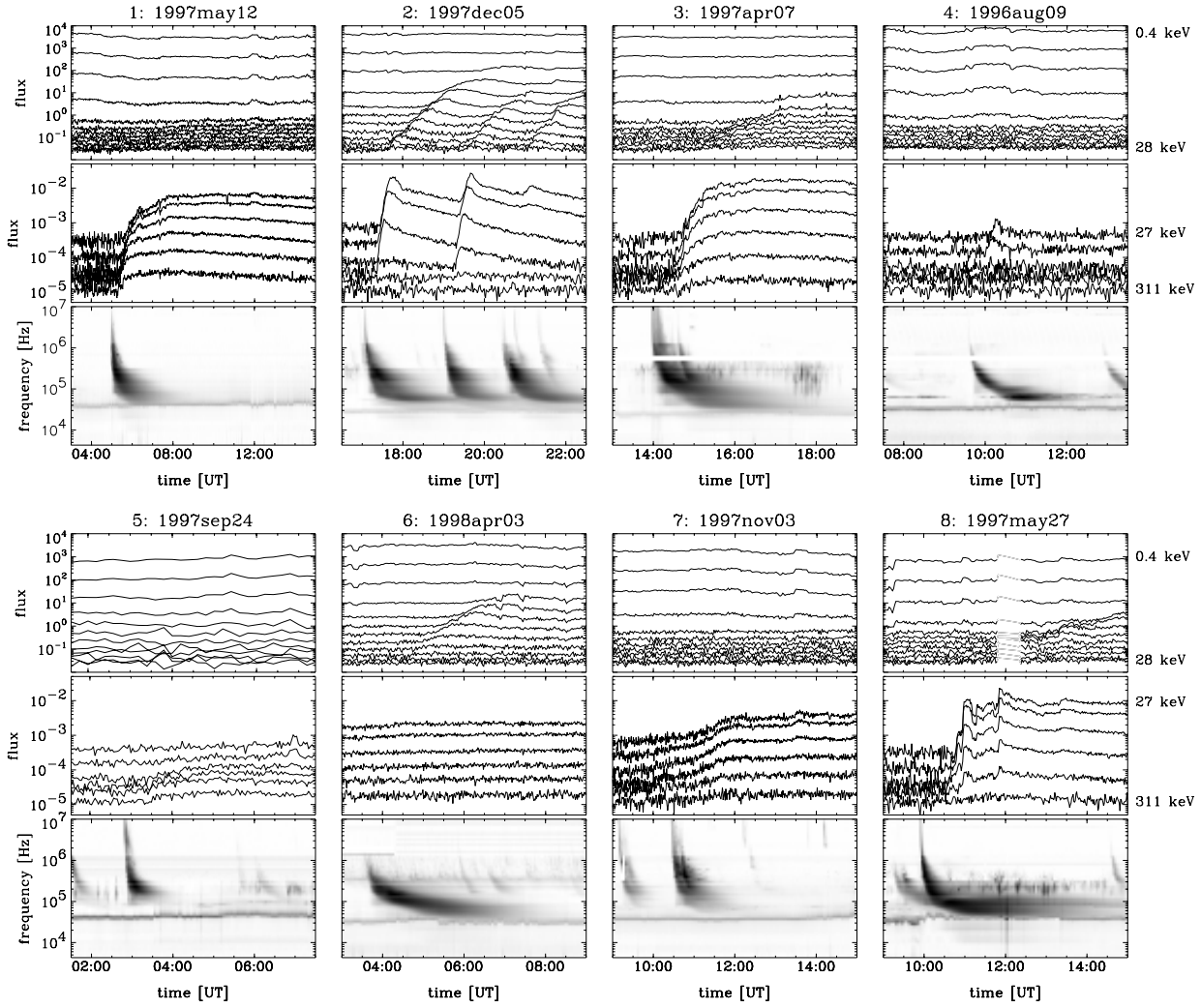

FIG. 1.—Overview plots of eight impulsive electron events. For each event, the two top panels show the observed electron flux at 1 AU: the top panels for the energy range of 0.4 (*top curve*) to 27.7 keV (*bottom curve*) and the middle panels for 26.8 (*top curve*) to 31 keV (*bottom curve*). In the bottom panels the radio spectrograms observed by *Wind* Waves instrument (Bougeret et al. 1995) are displayed. The dark areas are enhanced emission. For an easier comparison between these events, the time periods shown are equal in length (6 hr) and the flux and frequency axes are the same for all events. Starting at the top right, the events can be described as (1) event only at high energies; (2) multiple events down to energies around 1 keV; (3) event similar to event 1, with an additional weak enhancement at low energies; (4) weak event observed only at two energies; (5) very weak event at high energies; (6) event only at low energies; (7) complex event; and (8) solar event with no clear velocity dispersion.

are observed at energies above 25 keV, and since an accurate temporal analysis at energies below 25 keV is possible only for 12 events, two surveys are presented: one for events above 25 keV and one that includes only events detected also at lower energies.

In § 2, the data selection process is discussed, and is followed by the description of the approximation to the electron release time at the Sun of electrons producing the impulsive events at 1 AU (§ 3.1). The determined release time of electrons above 25 keV is then compared to the onset of the radio type III bursts (§ 3.2). Besides the temporal correlations, the spatial correlations between the flare site and the footpoint of the magnetic field lines connecting the Sun and the spacecraft are presented. For events with a high enough signal-to-noise ratio, a comparison of the release time at low energies is possible (§ 3.2.3). Proton events related to impulsive electron events are discussed in § 3.3. As a further possible candidate for the origin of the observed electrons, the temporal and spatial correlations with "EIT waves" are investigated (§ 3.4).

2. INSTRUMENTATION AND DATA SELECTION

The *Wind* 3-D Plasma and Energetic Particle (*Wind* 3-DP) experiment was designed to provide full three-dimensional measurements of electron and ion distributions (Lin et al. 1995). The energy range of solar wind and suprathermal electrons (3 eV to 300 keV) is covered by electron electrostatic analyzers (EESA-L and EESA-H) and solid state telescopes (SST). Standard *Wind* software has been used to calibrate and analyze the data. The presented flux curves were produced by summation over angular bins. The three-dimensional capability of the instrument made it possible to avoid summing over bins contaminated by solar soft X-rays or other background.

The search for impulsive electron events was first done automatically by using cross-correlation techniques. Solar events are expected to show a velocity dispersion. The temporal cross-correlation of different energy channels of dispersive events therefore shows a maximum at lag different from zero. Hence, the shift of the maxima in the cross-

correlation function can be used to find impulsive electron events. In a second step, the results of the automatic search were checked by going through all observations again by eye.

A survey of impulsive electron events observed in the first year of operation of the *Wind* 3-D plasma instrument was published by Ergun et al. (1998). In Figure 1, examples of typical impulsive electron events are presented. The observed velocity dispersion in electron events detected at 1 AU is a clear identification of a solar event. However, some of the most probable solar events, as for example event 8 in Figure 1, show no clear dispersion. The lack of dispersion may be explained by the crossing of boundaries of spatial structures by the spacecraft relative to the streaming electrons. The late rise time of the electron flux relative to the type III radio burst as observed in event 8 supports this assumption. Events 1–6 in Figure 1 represent the most common impulsive electron events: some are observed only at higher energies, some can be seen below 1 keV; others are rather weak, with only two or three energy channels showing an enhanced flux; and some events show no significant electron flux at energies above 10 keV. Less common events are given by events 7 and 8: some events show multiple enhancement with no clear onset (event 7), and others have no clear dispersion, as mentioned above.

For the statistical surveys, data from the past 3 yr of observations (1994 December through 1997 December) were used, but only events with the following properties were selected:

1. A clear velocity dispersion.
2. A good enough time resolution and a high enough signal-to-noise ratio (which are needed for an accurate determination of the start time).
3. An unambiguous start time. Complex events were therefore often not considered.

Hence, only events similar to events 1 to 6 in Figure 1 were selected. At energies above 25 keV, the above properties limit the number of investigated events to 58, whereas at lower energies the lower signal-to-noise ratio allows an accurate temporal analysis at high and low energies in only 12 events. For all these events, interplanetary and/or coronal type III radio bursts are observed. The larger number of events seen at high energies favors analysis of these events first; in a second step, the electron release time at lower energies is compared to the release of electrons above 25 keV.

Compared to *ISEE 3* observations (Potter, Lin, & Anderson 1980; Lin 1985), the different numbers of events seen only at energies below 15 keV is conspicuous: 40% of all events observed by *ISEE 3* during solar maximum are seen only at low energies, whereas for the *Wind* observations taken during solar minimum, events seen only at low energies are rare (Ergun et al. 1998). A comparison of the signal-to-noise ratios of the instruments aboard the *ISEE 3* and *WIND* spacecraft shows that the instruments of both missions have a similar sensitivity. Therefore, the occurrence rate of events seen only at low energies seems to be solar-cycle dependent.

3. DATA ANALYSIS AND DISCUSSION

3.1. *Electron Release Time*

The goal is to determine the release time at the Sun of the electrons observed at 1 AU. The temporal correlation of the release time with solar flares may then identify solar events associated with impulsive electron events. The release time of electrons with energy ϵ at the Sun, $t_0(\epsilon)$, can be approximated from the observed rise time of the electron flux at 1 AU, $t_{\rm AU}(\epsilon)$, and the time of flight, $\tau(\epsilon)$, it needs to travel from the Sun to the spacecraft:

$$t_0(\epsilon) = t_{\rm AU}(\epsilon) - \tau(\epsilon) = t_{\rm AU}(\epsilon) - \frac{L}{v_{\rm rel}(\epsilon)}\,, \qquad (1)$$

where L is the path length from the electron release site on the Sun to the spacecraft and $v_{\rm rel}(\epsilon)$ is the relativistic velocity of electrons with energy ϵ. In the next section, the approximation of $t_{\rm AU}(\epsilon)$ is discussed, followed by description of the determination of the most probable energy of electrons detected in an energy bin, and finally the approximation of the path length is explained.

3.1.1. *Determination of the Start Time*

Similar signal-to-noise ratios for all analyzed events allow us to determine all events with the same method without introducing possible systematic errors in the data analysis due to the different intensities of the events. Therefore, weak and noisy events were first integrated in time to have signal-to-noise ratios similar to those of the strongest events (with less temporal resolution, of course). Then the background was subtracted and the curves were normalized in units of standard deviations. For each of these time series, an upper limit of the start time, $t_{\rm upper}$, was determined by the first time with a background subtracted flux above 4 σ (see Fig. 2*a*). For even later times than $t_{\rm upper}$, the event has definitely started. The start time, $t_{\rm AU}$, was then chosen as the earliest of all relative to the $t_{\rm upper}$ preceding time step with a positive flux. The difference between $t_{\rm upper}$ and $t_{\rm AU}$ is used as an approximation of the uncertainty, $\delta t = t_{\rm upper} - t_{\rm AU}$. δt is an upper limit of the uncertainty and should not be understood in the same way as an uncertainty given by a standard deviation. The method discussed above could be done automatically. To check the results, all start times and their uncertainties were also determined by eye. The results were consistent.

3.1.2. *The Most Probable Energy of Electrons Detected in an Energy Bin*

The energy, ϵ, is given by the energy range of the different energy channels of the instrument. Within each bin, the most probable energy of electrons producing the rise phase of the event would be a good approximation for ϵ. However, there are two competing mechanisms influencing this value: (1) Because of the velocity dispersion, the first electrons to arrive in an energy bin have energies close to the highest energy in the bin. (2) The energy spectra are observed to be power-law functions with negative indices, which indicates that most of the electrons detected within an energy bin have energies close to the lower end of the energy range. Hence, the noise is determined by the numerous electrons detected near the lower limit of the energy range in a bin. The first arriving electrons detected at the highest energies in a bin may therefore not be numerous enough to produce a significant flux enhancement above the noise. The observed rise phase may in these cases be produced by the larger number of electrons at lower energies. Depending on the properties of the event, the most probable energy of electrons producing the rise phase can therefore be different than the highest energy in the bin.

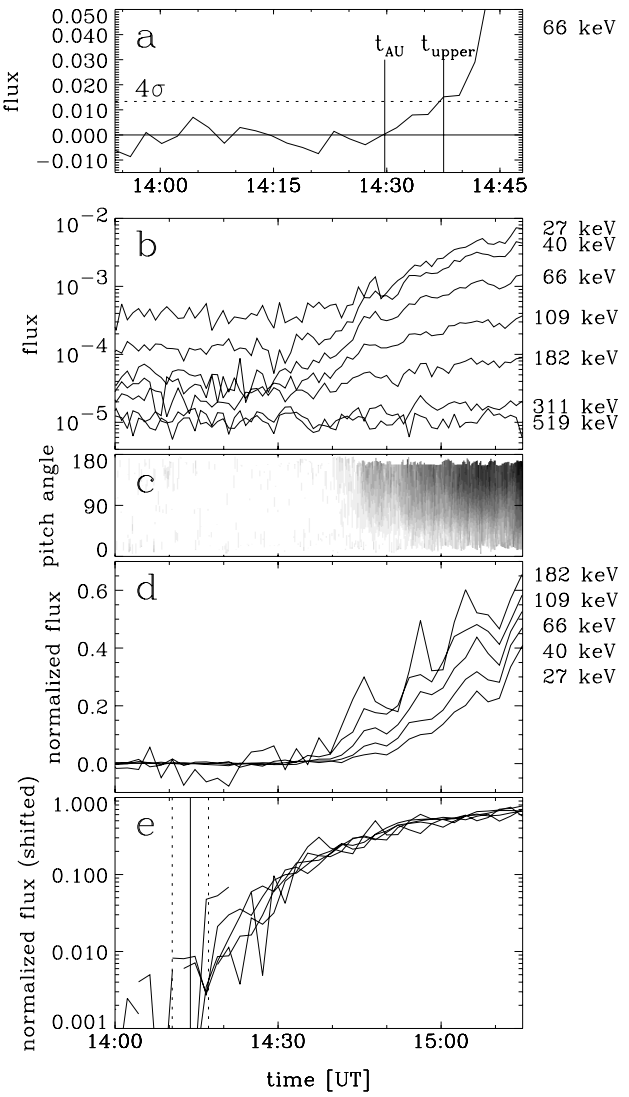

FIG. 2.—Example of the data analysis: (*a*) The background-subtracted time profile of the electron flux at 66 keV is shown to illustrate the determination of the start time and its uncertainty (see § 3.1.1). The dotted line shows the 4 σ level. The determined start time, t_{AU}, and the upper limit, t_{upper}, are marked. (*b*) An impulsive electron event observed on 1997 April 7. Only the first hour of the event is shown (see Fig. 1). (*c*) Pitch angle distribution for 40 keV electrons. The observed flux is shown in a gray-scale image of time and pitch angle. The dark area is enhanced flux. Electrons with pitch angle around 180° arrive first. (*d*) The normalized time profiles are shown in a linear scale. The velocity dispersion is obvious. (*e*) The shifted time profiles, for which the dispersion has been removed, are plotted . Within the accuracy, the curves at different energies lie on top of each other, indicating a simultaneous release at different energies within some minutes. The solid vertical line shows the approximated electron release time at the Sun, t_0, and the uncertainties in t_0 are shown by the dotted lines.

For energies above 25 keV, the additionally introduced uncertainties of $t_0(\epsilon)$ due to the uncertainties of ϵ are not larger than the uncertainties from the determination of the rise time, $t_{AU}(\epsilon)$. The difference in time of flight for the extreme values of the energy in a bin is about 200 s for energies above 25 keV. This value is comparable to or smaller than the determined uncertainties of the observed rise times.

For the analysis of the 58 events detected above 25 keV, the minimum value in each energy bin has been used as an approximation of ϵ, providing an upper limit of $\tau(\epsilon)$ and, therefore, an earliest possible release time. The later delays introduced between the type III onset time and the release time of the electrons producing the impulsive events are therefore lower limits.

At energies around 1 keV, the difference in $\tau(\epsilon)$ for the extreme values of the energy in a bin is around 20 minutes. During a that long time period, most of the events already show a significant flux enhancement relative to the background. Hence, at lower energies, the highest energy in a bin is a good approximation for ϵ. Therefore, in § 3.2.3, where the release time of events seen also at energies below 25 keV is investigated, the higher limit of the energy range in a bin is used as an approximation of ϵ.

3.1.3. *Determination of the Path Length*

The electrons are known to travel along the interplanetary magnetic field lines. The observed pitch angle distributions of impulsive electron events always show that the first arriving electrons are ones with pitch angle around 0° or 180° (see Fig. 2*c*), i.e., the first arriving electrons are traveling along or against the magnetic field lines. Therefore, the length of the magnetic field line from the Sun to the spacecraft can be used as an approximation of the path length.

The magnetic field in interplanetary space can be approximated by a Parker spiral. The only variable input in the calculation of the Parker spiral is the solar wind speed. Daily averaged values of the wind speed determined from *Wind* observations have been used to approximate the Parker spiral. The length of the field lines of the Parker spiral are then used as an approximation of L. The magnetic field configuration can vary significantly from a Parker spiral and might therefore introduce a systematic error in the determined path length. The observed velocity dispersion can be used as a test of the validity of the approximation, as shown in the following section.

3.1.4. *Summary*

After approximating the path length, the relative start of the electron release at the Sun at different energies can be investigated. First a background was subtracted from the observed fluxes and the fluxes were normalized to unity for each energy channel (see Fig. 2*c*). The velocity dispersion can be seen best in these curves. Then the time profiles were shifted according to the approximated time of flight, $\tau(\epsilon)$. The normalized and shifted curves for one event are shown in Fig. 2*d*. Within an accuracy of some minutes, the shifted curves show the same onset time. The dispersion seems to be removed. This indicates that the approximation of the path length is good and that electrons at different energies seem to be released simultaneously. The case where an energy-dependent release time would just compensate the incomplete correction for the dispersion, i.e., a bad approximation of L, is rather unlikely. For all investigated events, the results are similar to the one shown in Figure 2.

For each event and energy channel, the electron release time at the Sun, t_0, was determined. Within the uncertainties, the energy release occurs simultaneously at different energies. To improve the accuracy of t_0, an averaged electron release time was calculated by averaging over the release time at different energies. Averaged over all events, the uncertainties are 231 s.

3.2. *Comparison with Radio Type III Bursts*

3.2.1. *Temporal*

The onset time of coronal radio type III bursts, t_{III}, were collected from radio observations in the meter range as reported by Solar Geophysical Data. To be sure about the identification, the onset times determined from coronal type III bursts were compared with the onset time of the radio emission observed at 14 MHz by the *Wind* Waves experiment (Bougeret et al. 1995). The uncertainties in t_{III} are maximally ± 100 s, often much less, and in any case, they are smaller than the uncertainties in t_0.

Figure 3 shows the distribution of the electron release time, t_0, relative to the onset of the type III bursts, t_{III}. This distribution is uniform in $t_0 - t_{III}$. The approximated uncertainties, δt, allow us to distinguish roughly between simultaneously released events ($|t_0 - t_{III}| - \delta t < 0$) and delayed events ($|t_0 - t_{III}| - \delta t > 0$). Since δt is only a rough approximation, some events might be selected in the wrong group. However, electrons producing the impulsive events at 1 AU are released simultaneously within uncertainties (*solid curve*) or are delayed for up to 2000 seconds (*dashed curve*) relative to the release of the type III–producing electrons. A delay of 2000 s is of the same order of magnitude as the time of flight, $\tau(\epsilon)$, at these energies. In 29% ($\pm 7\%$) (17 of 58) of the events, the electrons producing the type III burst and the ones producing the impulsive events are released together and therefore most probably belong to the same population. However, in the majority of events, the impulsive electron events seem not to be directly related to the population of electrons producing the radio type III bursts. Another way to investigate this discrepancy is to look at the spatial correlation of the flare location and the footpoint of the magnetic field lines connecting the Sun and the spacecraft.

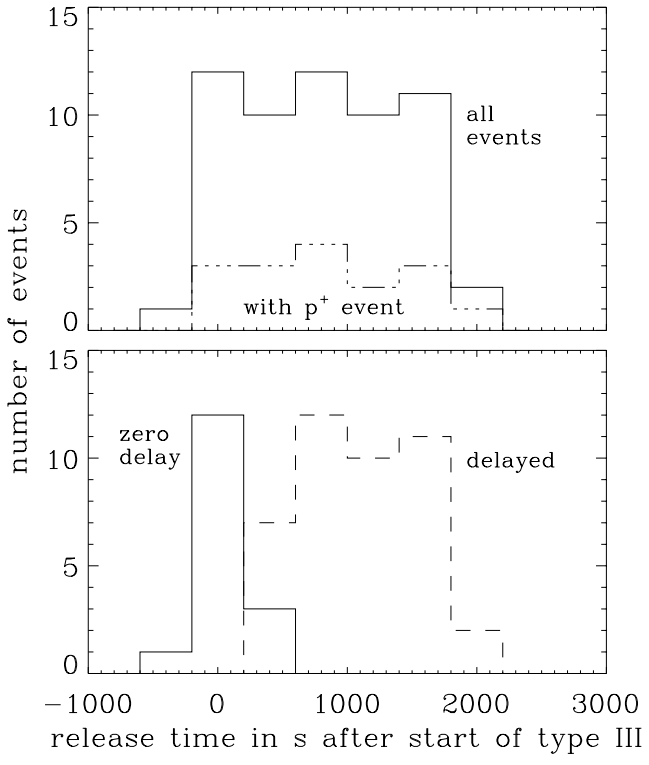

FIG. 3.—Distributions of electron release times. Zero on the time axis corresponds to the onset time of the type III bursts at the Sun. The top panel shows the distribution for all events (*solid line*). The bottom panel plots the distributions for events compatible within uncertainties with a simultaneous release (*solid line*) and events delayed (*dashed line*) relative to the start of the type III radio burst. Electron events with an additionally enhanced proton flux (see § 3.3.2) show a similar distribution as for all events (*top*, *dash-dotted line*).

3.2.2. *Spatial*

In this section, the spatial location of the flare site and the footpoint of the magnetic field lines connecting the spacecraft and the Sun are compared. For the events released simultaneously with a type III burst, it is expected that the flare site, i.e., the origin of the type III burst, is magnetically connected to the spacecraft. For events with a large delay, the relative location of the flare site and the magnetic footpoint may help to explain the timing.

The flare locations were determined by Hα and soft X-ray (SXR) observations. Solar Geophysical Data reports Hα flares for 26 of the 58 impulsive electron events. By looking for the strongest flarelike brightenings in *Yohkoh* SXR full-disk images, another 20 flare sites could most likely be determined. The strongest flarelike brightening is most probably related to the flare producing the type III radio burst. However, the possibility that an incorrect flare location was chosen for some events cannot be excluded. An additional problem is that some flare locations might be situated behind the limb. For the remaining 12 events, no *Yohkoh* data are available, and in four of these 12 events, the *GOES* data show no enhancement. This result is compatible with earlier studies of impulsive electron events that also found no related SXR flare for some events (Bothmer et al. 1997). However, the lack of SXR emission could also be explained by the detection limits of *GOES* or by flare locations far behind the limb.

The magnetic connection of the spacecraft with the Sun is more difficult to determine than the flare location. Assuming that the interplanetary magnetic field can be described by a Parker spiral, the footpoints of the magnetic connection are expected to be connected to western longitudes. However, the magnetic field configuration within some solar radii can vary significantly from the Parker model. On average, the connection may still be most probably centered around W60. The latitude of the magnetic connection is even more complicated and inaccurate. Hence, the location of magnetic connection is not well known, and the uncertainty in distance along the solar surface might be up to half a solar radius.

Figure 4 (*top*) shows the location of the flare sites (*diamonds*) on the solar disk. Additionally, the east-west coordinates of the approximated footpoints are given by the curves along constant longitudes. The distributions in longitude of these location are presented below. The approximated footpoint locations of the Parker spiral are around W60, with scatter of $\pm 30°$. The distribution of the flare sites also shows most of the locations around these longitudes. However, the distribution is broader, and several flares are even observed to occur on the eastern side of the solar disk. The distribution is asymmetric. There is no obvious reason for an asymmetry. It rather suggests that there are flares occurring behind the limb that are, therefore, not observable in SXR. For a symmetrical distribution, the expected fraction of flares behind the limb would roughly agree with the observed fraction of impulsive electron events with no observed SXR flare emission. Hence, it is likely that the

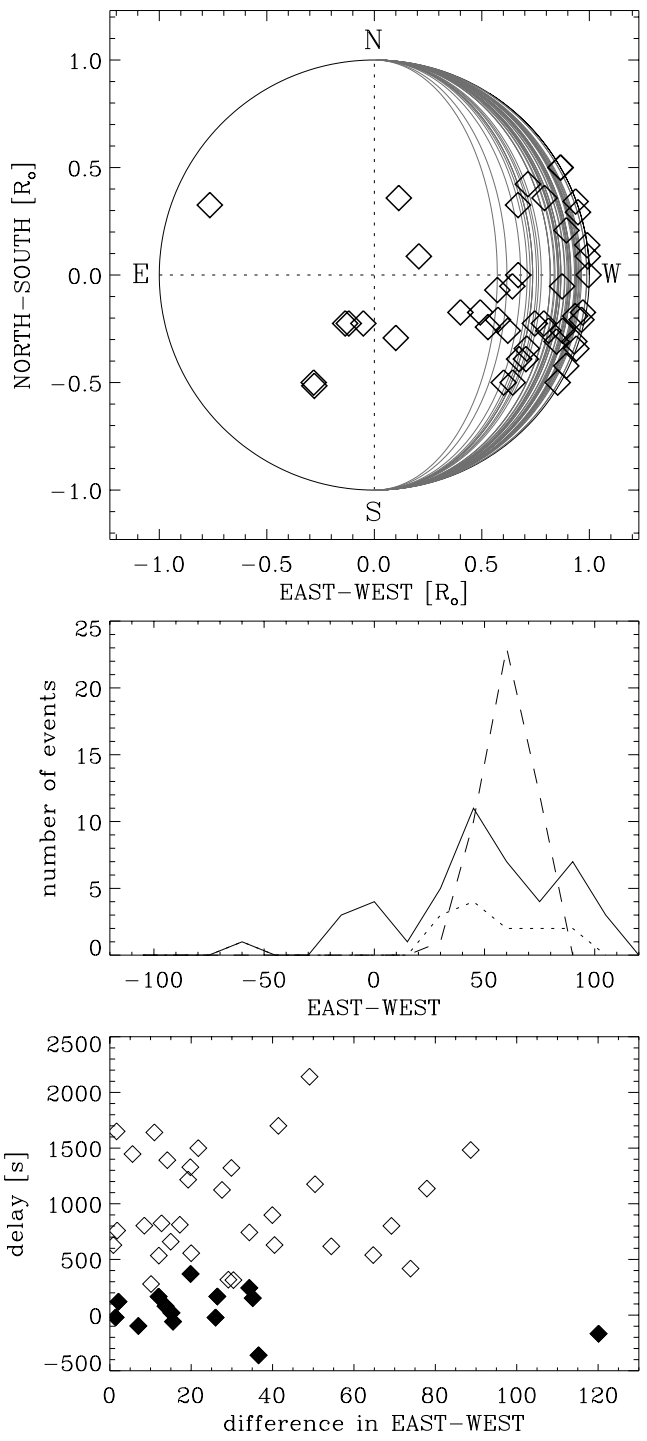

FIG. 4.—Spatial correlations. *Top*: The flare sites (*diamonds*) are shown on the solar disk. Curves along constant longitudes show the location of the magnetic footpoints connecting the Sun and the spacecraft, assuming that the magnetic field can be described by a Parker spiral. *Middle*: Distributions in longitudes for all flares (*solid line*), for events that are compatible with zero delay (*dotted line*), and for the footpoints of the Parker spiral (*dashed line*). *Bottom*: The delay, $t_0 - t_{III}$, is plotted as a function of the longitudinal differences between the flare sites and the footpoints of the Parker spiral. Black symbols mark events compatible with zero delay.

impulsive electron events without an observed SXR flare are related to unobservable flares occurring far behind the western limb.

The observed time delay between the electron release time and the type III onset, $t_0 - t_{III}$, can now be correlated with the distances between the flare location and the footpoints of the Parker spiral. Since the latitude of the location of the footpoint is difficult to approximate, only a comparison in longitude is presented (Fig. 4, *bottom*). Including the separation in latitude, the distances might be substantially larger. The events that are compatible with zero delay, are shown in black in Figure 4 (*bottom*). The magnetic footpoints connecting the Sun and the spacecraft of these events are expected to be close to the flare site. For all except one, the difference in longitude is smaller than 40°. Considering the large uncertainties, values up to 40° at least are not in obvious contradiction with the flare site being magnetically connected to the spacecraft. On the other hand, there are also many events within a longitude separation smaller than 40° with a delay significantly different from zero. However, the plot shown gives only the separation in longitude.

3.2.3. *Comparison with Onset Times at Lower Energies*

Until now, only the release time of electrons above 25 keV has been discussed. However, impulsive electron events are observed at energies down to 0.5 keV. The release time at lower energies has been excluded so far because of the lower signal-to-noise ratio at these energies and because several events show no significant enhancement at energies below 25 keV. In this section, the energy release time at high energies ($\geq$25 keV) are compared to the release time at low energies ($\leq$25 keV). The main question to answer is whether the electron release times are the same for all energies. A different behavior at different energies might also indicate a different origin and acceleration mechanism.

The signal-to-noise ratio at lower energies makes an accurate determination of the release time possible only for the largest events. An additional problem of the analysis of electron fluxes around several keV is that the background flux may vary significantly during the time of flight of electrons at these energies. A sudden increase in background flux, as for instance observed during boundary crossings, makes it difficult to determine the onset time of the solar event. To avoid difficulties with these problems, the onset times at lower energies were determined by eye.

A total of 12 events occurring during 1994 November and 1998 July with high enough signal-to-noise ratios were analyzed. For these events, an additional approach has been used to approximate the release time. The path length and the electron release time were determined by fitting a straight line to the rise time, t_{AU}, as a function of v_{rel}^{-1}. The slope of the fitted line gives the path length, L, whereas the intersection provides the solar release time, t_0 (see eq. [1]). Compared to the method previously described, this approach fits two parameters (l and t_0) instead of just one (t_0). The main reason to abandon the second approach for events seen only above 25 keV was the large uncertainties in the fitted parameters, which were introduced mainly by the small range of values of v_{rel}^{-1}. However, within the accuracy, both methods provide consistent results.

For the 12 analyzed events seen at low energies, three different cases can be distinguished (see Fig. 5): (1) In the most common case (seven of 12 events), a single straight line can fit the data over the entire inverse velocity range, and the determined release time is compatible with the release time of the type III radio burst ($t_0 \approx t_{III}$). (2) For three events, the data can also be fitted by a single line, but the determined electron release time is delayed relative to the

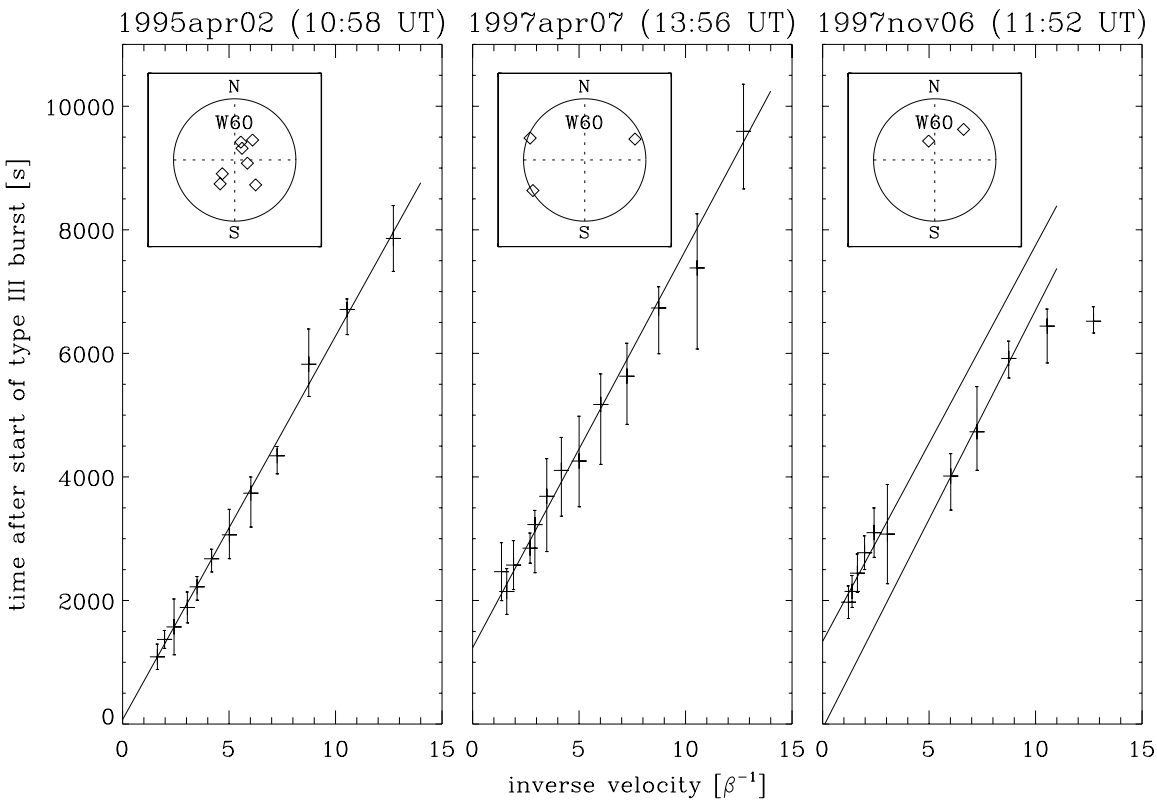

FIG. 5.—Start time of solar events observed at 1 AU as a function of inverse velocity is shown. The origin of the time axis corresponds to the start of the type III radio burst. The shown error bars are to be understood as maximal uncertainties. The straight lines are linear regressions to the observations. The slopes of these lines correspond to the path length, and the intersections give the solar electron release time. Three different cases are observed: (*left*) same release time for all electrons as for the type III burst ($t_0 \approx t_{III}$); (*middle*) same release time for all electrons but delayed relative to the type III burst ($t_0 > t_{III}$); (*right*) mixed case: low energetic electrons are synchronous with the type III burst, but high-energetic electrons are delayed. The inserts show the flare locations relative to the footpoint of the Parker spiral for events belonging to the same class. The shown solar disk is rotated such that the straight dashed line connecting the poles shows the longitude of the footpoint of the Parker spiral connecting the Sun and the spacecraft ($\approx$W60). Events with $t_0 \approx t_{III}$ are all relatively close to the approximated footpoint position, whereas the three events with a delay ($t_0 > t_{III}$) occur all far away from the footpoints of the Parker spiral.

type III start ($t_0 > t_{III}$). Electrons related to the radio type III burst seem not to be detected, which indicates that the spacecraft does not cross the trajectory of the type III–producing electron beam. (3) In the two remaining events, the observed values of $t_{AU}(v_{rel}^{-1})$ cannot by fitted by a single straight line alone: at both high (>25 keV) and low (<25 keV) energies, the data can be fitted by separated straight lines with the same slope, but different intersections. In these events, low-energetic electrons seem to be released simultaneously with the type III burst, whereas high-energetic electrons are released later. The third case can be interpreted as a combination of the previous ones.

The relative locations of the related flare site to the footpoint of the Parker spiral connection, the Sun, and the spacecraft also show different behavior for these three classes of events. For events with $t_0 \approx t_{III}$, the flare sites are observed to be relatively close to the approximated footpoint position, whereas for the three cases with a large delay ($t_0 > t_{III}$), the flare sites are at least 1 $R_\odot$ one away from the footpoint of the Parker spiral. This is consistent with the idea that radio type III emission-producing electron beams originating from the flare site reach the spacecraft only if the flare site is well connected with the spacecraft. For the events with a large delay ($t_0 > t_{III}$), the type III–producing electron beam travels along magnetic field lines not connected to the spacecraft.

3.3. *Proton Events*

The occurrence of proton enhancements during impulsive electron events may additionally help to distinguish different kinds of impulsive electron events. The *Wind* 3-D experiment also provides proton flux observations. The highest energy channels (1–7 MeV) were used to look for related events. The velocity dispersion can be used to select solar events related to the impulsive electron events. The solar release time of protons can be approximated in the same way as for electrons (see § 3.1). However, the signal-to-noise ratio is not sufficient to determine the timing relative to the electron release better than to within about 1 hr. In the sections below we will focus mainly on the following: first, we will investigate which electron events show an additional enhancement in the proton flux; then, in a second step, correlations with the observed delay between the start of the type III burst and the electron release are discussed.

3.3.1. *Flux Correlations*

Two different classes of solar electron events have been defined by the SXR burst duration, d_{sxr}, of the related flare emission: Cane, McGuire, & von Rosenvinge (1985) found that impulsive events ($d_{sxr} < 1$ hr) and long-duration events ($d_{sxr} > 1$ hr) show different characteristics, including a higher electron-to-proton ratio for long-duration events. In spite of the fact that Cane et al. selected larger events at

much higher energies (>3 MeV) observed during solar maximum, the same definitions have been used in the analysis of related SXR emissions in this work to allow a later comparison of results. Figure 6 (*left*) shows the *GOES* SXR peak flux (0.5–4 keV) as a function of the duration determined at 10% peak flux. *GOES* data were available for 56 electron events, and 46 events show flarelike enhancements, whereas for 10 electron events no clear SXR enhancement could be found. The determined durations of the related SXR emissions are rather short: there are only 15% long-duration events compared to 60% found in the data set by Cane et al., which indicates that electron events associated with a long-duration SXR emission seem to be less frequent at lower energies and/or during solar minimum. Additionally, no correlation between the duration of the SXR burst, $d_{\rm sxr}$, and the electron-to-proton ratio could be found. The different selection criteria, and therefore also the low number of long-duration events (three of the seven long-duration events show an enhanced proton flux), might be the main reason for these discrepancies.

In the survey of impulsive electron events around 25 keV, there seems to be rather a correlation between the SXR peak flux, $f_{\rm sxr}$, and the occurrence of an enhanced proton flux. For C class and larger flares, ($>10^{-6}$ W m^{-2}), the occurrence of related proton events seems much more likely to be observed. However, there are also three proton events with no related *GOES* SXR enhancements at all (no *Yohkoh* observations are available for these events). The absence might be again explained by a flare site behind the limb. *Yohkoh* full-disk images taken days before these flares show at least the existence of active regions behind the limb at the time the flares occurred. However, for all 3 days there are also active regions seen on the solar disk. A similar dependence is found for the electron peak flux instead of the SXR peak flux. Figure 6 (*middle*) shows the electron peak flux at 27 keV, f_{e^-}, as a function of the duration determined at half-peak flux. Proton events are observed only for electron events with duration longer than 1 hr and are more likely to occur for electron events with large peak flux. In conclusion, proton events related to impulsive electron events are more likely to be observed for large events in SXR as well as in electron flux. A second interpretation is that the absence of associated proton events in fainter events might be a question of instrumental sensitivity. This interpretation is supported by the fact that for increasing SXR fluxes, as well as for increasing electron fluxes, the proton fluxes, f_{p+}, also increase ($f_{p^+} \propto f_{\rm sxr}^{0.6}$ and $f_{p^+} \propto f_{e^-}^{1.0}$). However, there is a large scatter in these relations.

3.3.2. *Electron-to-Proton Ratio*

The first idea was that the occurrence of proton events during impulsive electron events may determine different classes of events. In the previous section, it was shown that the detection of a related proton event might rather be a question of sensitivity and that it is possible that all events have a related proton event. Some support for this is shown in the distribution of delays between the start of the type III radio burst and the electron release time. The distribution for electron events with related proton enhancements (Fig. 3, *top*, *dotted line*) is similar to the distribution for all events, which also show a uniform delay between zero and half an hour. It seems that the occurrence of proton events alone does not help to distinguish different classes of events.

The next step is to look for correlations between the characteristics of proton events and electron events. The observed delay between the onset of the type III burst and the electron release time at energies above 25 keV, $t_0 - t_{\rm III}$, seems to be the best place to look for correlations. For the 16 detected proton events, the electron events show a significant delay in 13 cases. Figure 6 (*right*) shows the correlation between the delay, $t_0 - t_{\rm III}$, and the electron-to-proton ratio determined from the total observed flux during the event. The events compatible with zero delay are marked by filled diamonds and on average show electron-to-proton ratios about an order of magnitude larger than events with a delay different from zero.

3.4. *Comparison with EIT Waves*

As shown in the previous sections, electrons that produce impulsive events at 1 AU often seem to be released later in the flare phase, especially at energies above 25 keV, and in some cases most probably also far away from the flare site. Nevertheless, impulsive electron events are most probably somehow related to flares. Flare-related phenomena

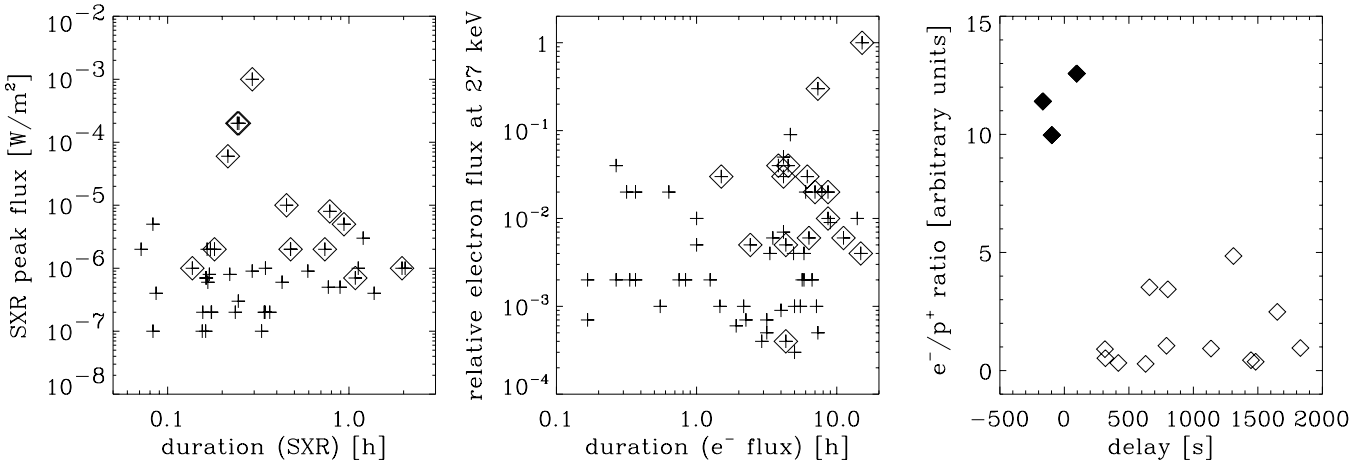

FIG. 6.—Statistics of proton events related to impulsive electron events. *Left*: The *GOES* SXR flux of flares related to impulsive electron events is shown as a function of the duration of the SXR emission. Diamonds mark electron events with enhanced proton flux. *Middle*: The same plot as on the left, but for the electron flux observed at 1 AU instead of the SXR flux. *Right*: The electron-to-proton ratio is plotted as a function of the delay between the start of the type III burst and the release time of electrons producing the impulsive events above 25 keV. Filled diamonds show events compatible with zero delay.

occurring later in the flare phase may therefore explain the origin of impulsive electron events. A primary candidate that might be related to impulsive electrons events is large-scale coronal disturbances (Thompson et al. 1998), as observed by the Extreme Ultraviolet Imaging Telescope (EIT) on board *SOHO* (Delaboudinière et al. 1995). These disturbances are observed in coronal iron line emission and are called EIT waves or coronal Moreton waves. Emanating from the flare site, a highly fragmented wave is observed to spread across the solar disk within less than 1 hr. Hence, the timescale is roughly of the same order of magnitude as the observed delays between the release time of the electrons that produce the impulsive events and the start of the flare. Additionally, the propagating wave may help explain how the flare site and the magnetic field lines between the Sun and the spacecraft are linked.

3.4.1. *Spatial and Temporal Correlations*

Simultaneous EIT observations are available for 29 of the 58 investigated impulsive electron events. The lack of simultaneous observations is mainly due to the later launch of the *SOHO* spacecraft. The EIT images used are taken in a bandpass dominated by emission from Fe XII lines. These lines are formed around 1.5 mK, which indicates a coronal origin of the emission. Since the emission is proportional to the density squared, the observed emission mostly originates from the lower corona (within $\approx 1.2\ R_\odot$). The average cadence of the images is around 15 minutes. Difference images have been used to look for large-scale disturbances. However, the identification of EIT waves is not always clear: The observed disturbances are rather weak and highly fragmented. Additionally, the temporal resolution is rather poor; and often only one image is available during the flare phase. In the following, the occurrence of an EIT wave is defined if there is a signature of a large-scale disturbance in at least one image. However, it is likely that some EIT waves are not detected because of sensitivity limits.

Events compatible with zero time delay (see Fig. 3) and events with a significant delay are investigated separately. Six of the 29 events with simultaneous EIT observations are compatible with zero delay and might therefore most probably be directly related to the radio type III bursts. In five of these six cases, no EIT wave was observed. For the 23 events with a significant delay, 17 events show EIT waves. In six of these 17 cases, the EIT data were good enough to follow the expansion of the EIT wave in time. These events were analyzed in more detail. The positions of the wave fronts at different times were determined by eye. Since the wave front is highly structured, the determined wave-front positions have to be understood as rough approximations.

The idea is now to interpolate the wave-front position at the time of the electron release, t_0, and to compare it with the footpoint of the Parker spiral connecting the Sun and the spacecraft. If the moving wave front reaches the footpoint at the time of the electron release, t_0, the observed impulsive electron event at 1 AU might be related to the EIT waves. Detailed temporal and spatial correlations are easier to do for flare locations near disk center. In these cases, the unknown latitude of the magnetic connection is not that important, and the wave front can additionally be followed as it moves over the solar disk. For flares occurring near the western limb, projection effects and the unknown latitude of the magnetic connection make a comparison difficult. For the three events with a flare site near disk center (Fig. 7, *top*), the correlation is unambiguous: at the time of the electron release, the wave fronts do not yet reach the footpoints of the Parker spiral connecting the Sun and the spacecraft. The speed of the wave front (≈ 350 km s^{-1}) is up to a factor of 2 too slow to connect the flare site with the magnetic connection. A similar result is reported by Bothmer et al. (1997) for the event on 1997 April 7, and they concluded that EIT waves are unlikely to be the source of electron events. For the other three events with a flare site near the western limb (Fig. 7, *bottom*), the geometry is less clear. Analysis of proton flux onset times of some of the above-mentioned events are reported by Torsti et al.; they estimate the solar release time of protons "to be close to the time when the Moreton wave approached the west limb" (1998, 2527). However, their accuracy does not allow a detailed temporal comparison.

All these comparisons of wave-front propagation were done using iron line emission originating from the lower corona. The determined wave-front positions are therefore the positions at lower altitude in the corona ($\leq 1.2\ R_\odot$). The comparison at these altitudes show that at least for the three unambiguous cases the wave front travels too slowly to reach the magnetic connection to the spacecraft. However, the electrons might be released at high altitude, where the wave front may move faster. A higher altitude, i.e., a low density in the electron release region, is also predicted by in situ observations (Lin 1985; Lin et al. 1996). To explain the escape of 1 keV electrons, the density in the release region has to be below an upper limit to allow a scatter-free escape in the interplanetary space. For an even higher density, the collision rate would be too high to allow an escape. An exponential density scale height and a temperature of 2 mK, the observed cutoff energy of ≈ 1 keV, as observed during the event on 1997 April 07 (see Fig. 1), predict an upper limit for the density in the electron release region of $5 \times 10^7 \mathrm{cm}^{-3}$. The highly fragmented structure of the corona makes it difficult to relate density to a well-defined altitude, but an electron release region between 1.2 and 2 $R_\odot$ seems to be most likely. Therefore, the observed wave-front positions seen in EIT images of the lower corona are probably not the ideal positions to which to compare the timing. Since the waves fronts are not observed at higher altitude, model computations of the propagation of hydromagnetic disturbances may help explain the wave propagation higher up in the corona.

3.4.2. *Propagation of Hydromagnetic Disturbances*

Computations of the propagation of hydromagnetic disturbances are presented by Uchida (1968). He studied these phenomena in an isothermal, spherical symmetric corona with a radial magnetic field in the WKB approximation. These are rough approximations. However, this model can be used as a first approach to the problem. Uchida found that an expanding fast-mode wave is propagating through the corona.

Uchida's calculation are repeated to model the location of the EIT wave at lower altitudes and are then used to investigate the wave-front propagation higher up in the corona. The free parameters are the temperature, T, and the Alfvén speed, v_A, at the bottom of the corona. Since the simplifications are large, a typical scenario approximated from the observations is modeled rather than each single event.

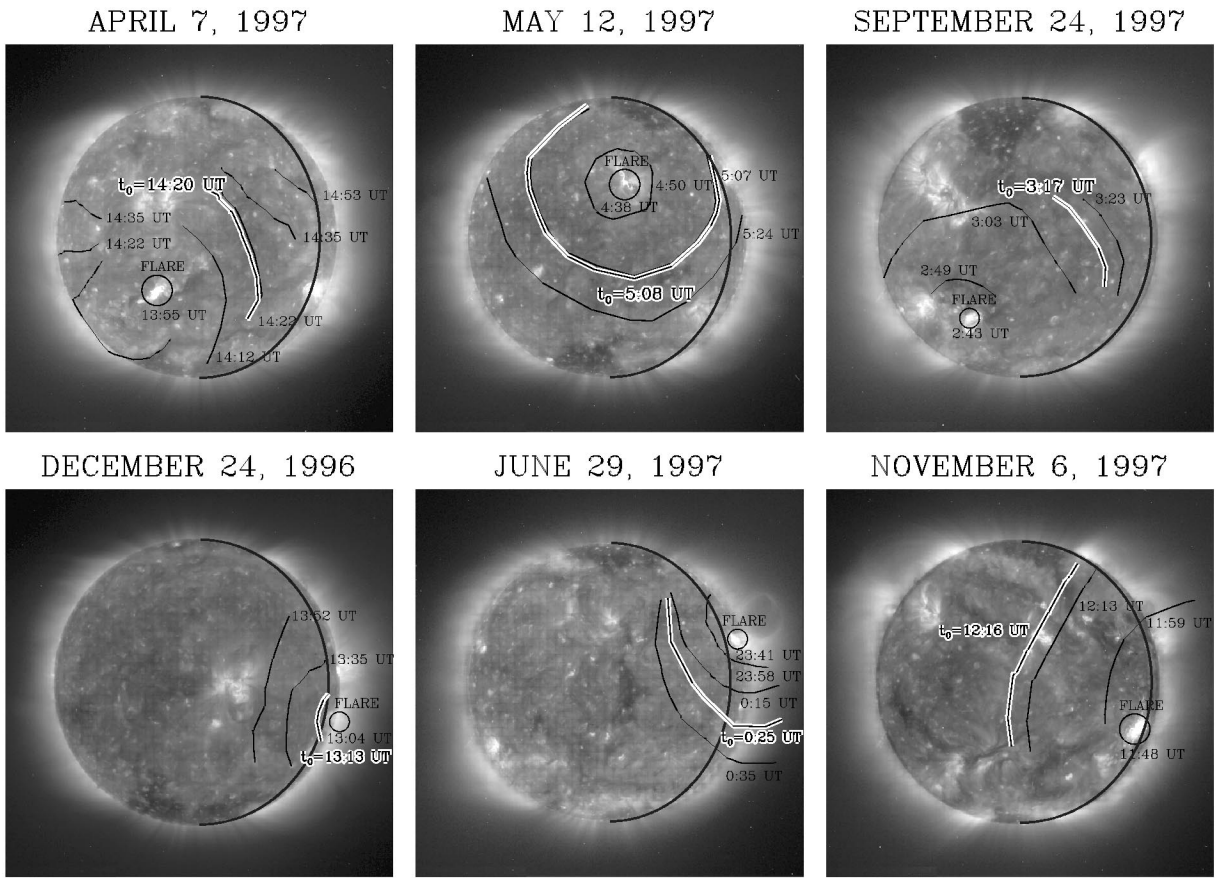

FIG. 7.—Coronal Moreton wave observations. The temporal evolution of the leading edge of the wave fronts outlined in black are plotted on the *SOHO*/EIT 195 Å image. The six events with the best temporal coverage are shown. The flare sites are marked by circles. The black and white curves give the interpolated wave-front position at the time of the electron release, t_0, whereas the black curves along constant longitudes are the expected footpoint locations of field lines connection the Sun and the spacecraft.

For $T = 1.5$ mK and $v_A = 2000$ km s^{-1}, the calculations show a quantitative agreement with the EIT observations (see Fig. 8): At lower altitude, the wave front moves with a speed of about 250 km s^{-1}, which is comparable to the observed speed of the EIT wave propagation. Because of the larger Alfvén velocity at higher altitude, the wave front moves faster at higher altitude. Assuming now the difference between the flare site and the footpoint of the Parker spiral to be around 1.2 $R_\odot$ and that the delay between the flare start and the electron release is roughly 1800 s, the calculated wave front at higher altitude is fast enough to connect the flare site with the field line connecting the Sun and the spacecraft. The connection would be at high altitude. The altitude of this connection strongly depends on the detailed magnetic field configuration and the density and temperature structure in the corona. However, values around 1.5 $R_\odot$ seem to be possible.

4. SUMMARY AND CONCLUSIONS

Two different kinds of signatures of electron beams escaping from the Sun into interplanetary space have been investigated: impulsive electron events and radio type III bursts. Comparisons of the solar release times of electrons producing these two signatures have been used to investigate whether impulsive electron events and type III radio bursts are produced by the same electron population or whether they originate from different populations. Timing analyses were done for 58 events at energies about 25 keV. The lower signal-to-noise ratio at energies below 25 keV restricts the number of analyzed events at these energies to 12 of the 58 events.

At lower energies (<25 keV), the release times of electrons producing radio type III bursts and electrons forming the impulsive events at 1 AU are equal within the uncertainties in nine of 12 events. For these events, it is most likely that the type III bursts and the impulsive electron events are produced by the same electron population. Spatial correlations of the most probable origins of these events also support this interpretation. At higher energies (>25 keV), the timing is different: in 41 of 58 events, the type III burst–producing electrons are generally released earlier. They are released in the impulsive flare phase, whereas the electrons forming the impulsive events at 1 AU are released up to 2000 s later. This fact makes it unlikely that both phenomena are produced by the same electron population. More importantly, it suggests that the low- and high-energy populations of interplanetary electron events do not originate from the same acceleration process. In several of these events, spatial observations show flare sites in the eastern part of the solar disk or well behind the western limb. A direct magnetic connection between these flare sites and the spacecraft is rather unlikely, which indicates that at least some of the impulsive electron events are most probably not directly related to the flare site where the

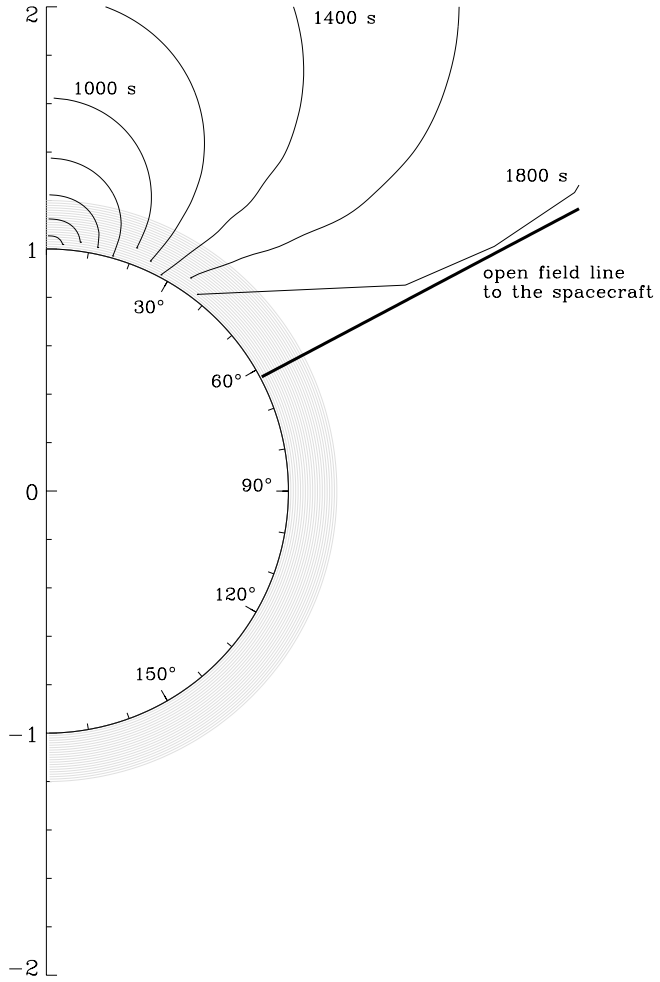

FIG. 8.—Model calculation after Uchida (1968). The source of hydromagnetic disturbances is located at the bottom of the corona at $\theta = 0°$, and the wave fronts expanding in time are shown as thin black lines. The temporal separation between the shown wave fronts is 200 s. The emission seen in the EIT images is expected to come from the lower corona shown in gray. The thick black line is assumed to be a field line connecting the Sun and the spacecraft.

type III–producing electrons are released. For events with a flare site in the east or far behind the western limb, the electron beams producing the type III bursts are most probably not crossing the spacecraft trajectory and are therefore only detected by the remote sensing radio observations.

The different timing at energies below and above 25 keV suggests that at least two different classes of impulsive electron events exist. One class of events (type III–related) is produced by the same electron population as the type III radio bursts, and the other class (not type III–related) is produced later by a different electron population at rather higher energies. However, there are also events that are type III–related observed down to 1 keV, which suggests that this class of events also has significant flux at low energies. At least two events clearly show that events of both kinds of classes can occur during the same solar flare. In these events, the type III–related electron events show a cutoff at high energies around 20 keV, and at even higher energies the electrons are released later and are therefore not related to the type III radio burst. Since the type III–related events generally occur earlier, both classes of events can be detected clearly only if the cutoff at high energies of the type III–related event is lower than the cutoff energy of the events that are not type III–related. This might partially explain the relatively low number of observed events that are not related to type III bursts at low energies.

Impulsive electron events observed at 1 AU seem to be produced by at least two different classes of electron beams escaping from the Sun into interplanetary space. One class includes electron beams producing radio type III emission related to the impulsive phase of the flare, and the other class is released later in the flare phase, escaping without emitting any observable radio emission. A major question now is why the second class of electron beams do not produce any radio signatures (type III bursts). The temporal delay after the flare-related type III bursts of up to 2000 s should make the detection of a second radio type III burst produced by the delayed-release electron beam easily possible in the centimeter to kilometer radio range. However, no such signatures are observed. There seems to be a major physical difference between the two groups of electron beams, so that one group produces radio emission and the other one does not. Drift rates of radio type III bursts suggest that electrons with energies between 2 and 30 keV are unstable electrons in a radio type III burst–producing electron beam. The lack of enhanced electron flux at these energies, as observed in some events, might be the reason for the absence of radio emission. The beam at higher energies may not be focused well enough to form an instable beam. However, more investigations are needed. In any case, the lack of radio type III emission in the second group of events should be considered when proposing acceleration mechanisms of these electron beams.

Coronal Moreton waves are investigated as another flare-related phenomenon possibly related to impulsive electron events. The long duration after the flare start (up to 1 hr) and the propagation of the event across the solar disk connecting large distances make these events useful for explaining the temporal and spatial behavior of the impulsive electron events relative to flares. For 75% of all impulsive electron events not related to type III bursts, signatures of coronal Moreton waves are observed. Temporal and spatial correlations show that the observed part of the wave fronts at low altitude in the corona are moving too slowly to connect the flare site and the footpoint of the most probable magnetic connection between the Sun and the spacecraft. However, hydromagnetic simulations suggest faster moving wave fronts higher up in the corona. The speed of wave fronts around 1.5 $R_\odot$ could be fast enough to link the flare site with the magnetic connection between the Sun and the spacecraft, which indicates a possible relation between Moreton waves and impulsive electron events. It would also indicate a high altitude for the electron release region, which would explain the scatter-free escape of electrons with energies of some keV. An open question is still the actual acceleration mechanism: the moving wave front may, for example, trigger the particle release, or it might be directly responsible for accelerating of the particles. However, since the nature of coronal Moreton waves is still not yet understood, it is difficult to favor any possibilities at the moment.

The existence of two classes of impulsive electron events is also supported by simultaneous proton flux observations. For impulsive electron events with large electron and SXR fluxes, an additional proton enhancement is often observed. The detection of an associated proton event might be

limited by instrumental sensitivity only, and it is possible that all events have associated proton events. However, impulsive electron events not related to type III radio bursts are observed to be proton-rich, showing electron-to-proton ratios about an order of magnitude lower than events related to type III bursts. The number of proton events occurring together with impulsive electron events related to type III bursts is only three. However, all of these events show electron-to-proton ratios higher than those of the other 13 proton events by at least a factor of 2.

SEP events can also be distinguished on the basis of whether they are proton-rich or proton-poor events. The classification of SEP events was originally based on the solar SXR burst duration of the related flare emission: impulsive SEP events are related to short-duration SXR bursts, and gradual SEP events are related to long-duration SXR bursts (see reviews by Reames 1995, 1997). Gradual SEP events are observed to be proton-rich and are therefore also called proton events, whereas impulsive SEP events are electron-rich and show additionally a very high ^{3}He-to-^{4}He ratio. Impulsive SEP events are flare-related, and gradual SEP events are associated with shock waves driven by coronal mass ejections (see Kahler et al. 1984). Delayed solar release times of events related to flare sites far in the east or behind the western limb are reported for proton events (see Reinhard & Wibberenz 1974). Reinhard & Wibberenz suggested a rapid transportation process in the initial phase after the flare fills up a so-called fast propagation region. Lin & Hudson (1976) first proposed the identification of this fast propagation region with the region over which a shock wave accelerates particles. The analogy to the type III–related and type III–unrelated electron events discussed in this work is obvious: impulsive and gradual SEP events could be identified with type III–related and type III–unrelated impulsive electron events, respectively. More investigations should be done to identify a possible relation. In particular, observations of simultaneously released ions and their compositions should help to characterize impulsive electron events.

We would like to thank S. D. Bale, A. O. Benz, and G. Mann for helpful discussions, and we wish to thank all of the individuals who contributed to the success of *Wind*. In particular, we would like to thank R. P. Lepping for providing *Wind* MFI data and J.-L. Bougeret for providing wind WAVE data. The 3-D experiment is a joint project of the University of California, Berkeley; CESR Toulouse, France; ESA/ESTEC, Noordwijk, the Netherlands; and the University of Washington. The WAVES experiments are joint projects of NASA/GSFC, Observatoire de Paris, CETP, and the University of Minnesota. *SOHO* is a joint project between the European Space Agency, ESA, and NASA. EIT was funded by CNES, NASA, and the Belgian SPPS. The work of S. K. is supported by the Swiss National Science Foundation and NASA grants NAG5-2815 and NAG5-6928 at Berkeley.

REFERENCES

Bougeret, J.-L. et al. 1995, Space Sci. Rev., 71, 231
Bothmer, V., et al. 1997, in Proc. 31st ESLAB Symposium, ed. A. Wilson (SP-415) (Noordwijk: ESA), 07
Cane, H. V., McGuire, R. E., & von Rosenvinge, T. T. 1986, ApJ, 301, 448
Feldman, W. C., et al. 1975, J. Geophys Res., 80, 4181
Delaboudinière, J.-P., et al. 1995, Sol. Phys., 162, 291
Ergun, R. E., et al. 1998, ApJ, 503, 435
Kahler, S. W., et al. 1984, J. Geophysical Res., 89, 9683
Lin, R. P. 1985, Sol. Phys., 100, 537
Lin, R. P., & Hudson, H. S. 1976, Sol. Phys., 50, 153
Lin, R. P., et al. 1995, Space Sci. Rev., 71, 125
Lin, R. P., et al. 1996, Geophys. Res. Let., 23, 1211
Potter, D. W., Lin, R. P., & Anderson, K. A. 1980, ApJ, 236, L97
Reames, D. V. 1995, Rev. Geophys. Suppl., 33, 585
———. 1997, in Geophysical Monograph 99, Coronal Mass Ejections, ed. N. Crooker, J. A. Joselyn, J. Feynman (Washington, DC: Amercan Geophysical Union), 217
Reinhard, R., & Wibberenz, G. 1974, Sol. Phys., 36, 473
Thompson, B. J., et al. 1998, Geophys. Res. Lett., 25, 2461
Torsti, J., et al. 1998, Geophys. Res. Lett., 20, 2525
Uchida, Y. 1968, Sol. Phys., 4, 30